

**Raman spectra of lithium doped single-walled 0.4 nm carbon nanotubes**

J. T. Ye, Z. M. Li, and Z. K. Tang\*

*Department of Physics and Institute of Nano Science and Technology, Hong Kong University of Science and Technology, Clear Water Bay, Kowloon, Hong Kong, China*

R. Saito

*Department of Electronic Engineering, University of Electro-Communications, 1-5-1 Chofugaoka, Chofu-shi, Tokyo 182-8585, Japan*

(Received 25 October 2002; revised manuscript received 13 December 2002; published 19 March 2003)

Using the vapor phase adsorption method, we show that it is possible to intercalate lithium atoms into 0.4-nm diameter single-walled carbon nanotubes. The charge-transfer behavior is studied by resonant Raman spectra. With increasing doping concentration, the radial breathing mode of these tubes shifts to higher frequency by about  $18\text{ cm}^{-1}$  because the vibration perpendicular to the tube axis is depressed. The *G* band exhibits conventional softening and downshift behavior. By decomposing the *G* band by one Breit-Wigner-Fano line shape and three Lorentzians, we found that the softening and downshift is due to the intensity competition between four components. The BWF component at  $1558\text{ cm}^{-1}$  couples with the electronic continuum and survives until the saturated doping stage.

DOI: 10.1103/PhysRevB.67.113404

PACS number(s): 78.30.Na, 63.22.+m, 63.20.Kr, 61.72.Ww

Modification of physical properties of carbon nanotubes by means of doping is of considerable interest.<sup>1,2</sup> By filling electrons into the electronic states, the Fermi level can be tuned to coincide with a van Hove singularity, leading to enhancement of conductivity or even superconductivity. Experimentally, the resistivity of carbon nanotubes doped with K or Br<sub>2</sub> decreases by a factor 20 or 30 at room temperature.<sup>3</sup> In Raman spectra, corresponding to the electron or hole doping is a spectral shift to lower or higher frequency of the graphitelike tangential modes. These shifts provide direct evidence for charge transfer between the dopants and tubes.<sup>2,4</sup> Bendiab *et al.* showed that there is a stable phase for intermediate doping level for alkali-metal doped single-walled carbon nanotubes (SWNTs), leading to the nonmonotonic behavior of the Raman spectrum.<sup>5</sup> In comparison with many attempts of alkali atoms intercalation in graphite and fullerene, doping lithium to nanotube is more attractive because carbon nanotube is expected to be a new efficient anode material for rechargeable Li-ion batteries. The alkali-metal storage capacity of SWNT bundles is higher than that of the graphite and disordered carbon.<sup>6</sup> Shimoda *et al.* showed that the reversible lithium storage capacity could increase from LiC<sub>6</sub> to LiC<sub>3</sub> when SWNTs were chemically etched to short segments.<sup>7</sup>

Some calculations for intercalation of alkali metal in small nanotubes have been carried out. Miyamoto *et al.*<sup>9</sup> have shown that a chain of K atoms exhibit an exothermic interaction with (7,0) and (8,0) tubes. First-principles local density function (LDA) calculations for the small (5,0) and (6,0) tubes indicated that doping K into them is not favorable because of their small diameter.<sup>10</sup> Of alkali dopants, lithium is the only candidate left which is thermodynamically and kinetically favorable for these small SWNTs.<sup>11</sup> Recently, ultrasmall 0.4-nm SWNTs were successfully synthesized inside the microporous zeolite AlPO<sub>4</sub>-5 (structure type code: AFI).<sup>12,13</sup> The SWNTs formed inside the channels are monosized and arrayed in a close-packed hexagonal lattice. The existence of the 0.4-nm nanotube has been confirmed by im-

age of transmission electron microscopy,<sup>12</sup> x-ray diffraction,<sup>14</sup> optical absorption spectra, as well as radial breathing Raman modes.<sup>15–17</sup> There are three possible chiralities for the 0.4-nm SWNTs; they are the zigzag (5,0), the armchair (3,3), and the chiral (4,2) tubes.

In this Brief Report, we report the Raman spectra of lithium doped 0.4-nm nanotubes. The 0.4-nm nanotubes are kept open as hydrogen atoms saturated the dangling bond during the pyrolysis process, which helps to maintain a favorable environment for lithium atoms to enter.<sup>11</sup> LDA calculation showed that there are three possible locations, as marked in Fig. 1, for intercalation of lithium atoms in the SWNT/AFI system: inside the nanotube (location 1), the interstitial space between the tube and the inner wall of the AFI channel (location 2), and inside the small six-ring channels (location 3). However, it has much higher energy for lithium

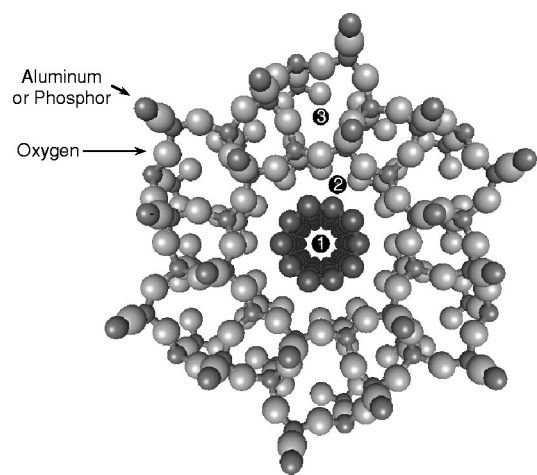


FIG. 1. Ball-and-stick model of the AFI single crystal containing a zigzag (5,0) tube. There are three possible locations for insertion of lithium indicated by 1, 2, and 3, respectively. First-principles calculation involving zeolite and tube shows that the third possibility is the smallest (Ref. 8).

to stay in location 3 in comparison with other two locations.<sup>8</sup> Especially, lithium atoms located inside the nanotube are favorable to line up as a single-atom chain, which leads to a very interesting structure: zeolite crystal forms a template for 0.4-nm carbon nanotubes that in turn served as templates for single lithium atomic chains.<sup>11</sup> There exists obvious charge transfer from lithium atoms in location 1 and 2 to the nanotubes. It is noteworthy that the superconducting fluctuation below 15 K has been observed in such ultrasmall nanotubes.<sup>18</sup> We expect that the mean-field critical temperature can be substantially increased by means of lithium intercalation. Thus controlling lithium concentration and evaluating the Fermi energy position in 0.4-nm SWNTs by Raman spectroscopy become an important subject.

Lithium is doped into the SWNT/AFI system by means of vapor phase adsorption. SWNT/AFI crystals are sealed together with pre-distilled lithium metal into a Pyrex glass tube under  $10^{-6}$  mbar, and then heated at 220 °C for 5 h. The lithium doped sample can be seriously destroyed immediately if exposed to air because of strong chemical reaction, especially at both ends of the AFI crystal, where the channels are open. In order to perform Raman measurements, a rectangular Pyrex tube with a  $2 \times 5$  mm<sup>2</sup> cross section is used. Unpolarized Raman spectra are measured at room temperature using a Renishaw 3000 micro-Raman system with a He-Ne laser (632.8 nm). A  $5 \times$  microscope objective is used to focus the laser beam and collect the scattered light. The laser spot has a diameter of 2  $\mu$ m. The spectral resolution is 1 cm<sup>-1</sup>. For the unsaturated sample, the lithium concentration is gradually decreased from the edge to center of the zeolite crystal, which provides us experimental facility to study Raman spectra at elevated doping concentration.

The resonant Raman spectrum is dominated by three features: radial breathing mode (RBM), the graphite-like *G* band, and the disorder-induced *D* band. In the regime of elastic approximation, the frequency of the RBM,  $\omega_{\text{RBM}}$ , scales inversely proportional to the tube diameter  $d_t$ .<sup>19</sup> Because of the strong curvature effect in 0.4-nm SWNTs,<sup>15,20–21</sup> however, the frequency of the RBM tends to deviate from the inverse relation. Calculation using the frozen phonon method showed that frequencies of three SWNTs are in order of  $\omega_{\text{RBM}}(5,0) < \omega_{\text{RBM}}(4,2) < \omega_{\text{RBM}}(3,3)$ , although geometrically  $d_t(5,0) < d_t(3,3) < d_t(4,2)$ .<sup>21</sup> Spectrum 0 in Fig. 2 shows the pristine RBM. It is dominated by two peaks at 510 and 550 cm<sup>-1</sup>, which are attributed to the (5,0) and (4,2) tubes, respectively.<sup>21</sup> The RBM of the (3,3) tube can be assigned to the shoulder near 580 cm<sup>-1</sup>, which is too weak to be identified from the background. This is possibly due to improper resonant condition, since optical transition energy of the (3,3) tube is 3.0 eV, much higher than the excitation energy.<sup>15</sup>

Lithium concentration gradually increases from spectrum 0 to 10 in Fig. 2. Both of the RBM lines show intensity loss. The RBM of the (5,0) tube even disappears in saturated doping stage (spectrum 10). That of the (4,2) tube shifts slightly to higher frequency in spectrum 6–10, which can be understood in terms of enhanced stiffness of the SWNTs upon lithium doping. Among the three tubes, the (4,2) tube has the largest diameter, thus more Li can enter and more deforma-

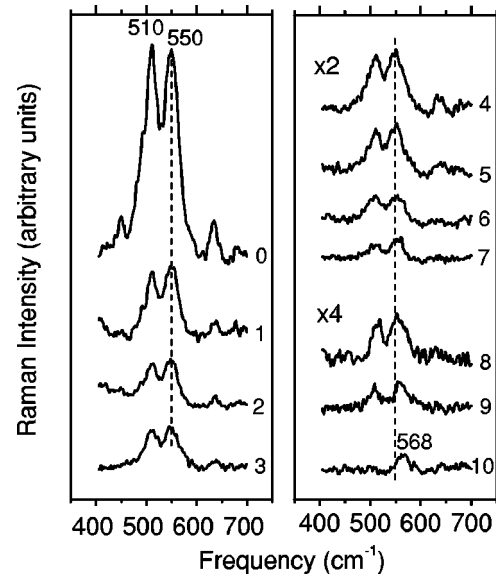


FIG. 2. Radial breathing Raman mode of lithium doped 0.4-nm SWNTs. From 0 to 10: pristine to saturated lithium doped sample. The dashed line denotes the RBM of pristine (4,2) tube which shifts from 550 to 568 cm<sup>-1</sup>.

tion of the phonon dispersion. The frequency upshift of the RBM mainly depends on the size of the dopant elements and its concentration. In spectrum 10, the RBM of the (4,2) tube shifts upward by 18 cm<sup>-1</sup>, in contrast with the large shift (74 cm<sup>-1</sup>) observed in Br<sub>2</sub> doped SWNTs.<sup>2</sup>

Based on polarization studies on SWNT bundles<sup>22</sup> and theoretical predictions,<sup>1</sup> the tangential *G* mode for a general chiral tube consists of modes of three symmetries: *A*, *E*<sub>1</sub>, and *E*<sub>2</sub>. Each of them further split into two lines denoted by *G*<sup>+</sup> and *G*<sup>-</sup> because of the curvature effect.<sup>23,24</sup> The upper frequency  $\omega_G^+$  located near 1600 cm<sup>-1</sup> is associated with carbon atom displacement along the tube axis, which shows very small diameter dependence. The lower frequency  $\omega_G^-$  is associated with carbon atom oscillation in the circumferential direction, which strongly depends on the tube diameter.<sup>24</sup> For the tube diameter from 0.9 to 3.0 nm, the separation between  $\omega_G^+$  and  $\omega_G^-$  can be fitted well with an exponential equation

$$\omega_G^+ - \omega_G^- = C/d_t^2, \quad (1)$$

where the constant *C* equals 47.7 cm<sup>-1</sup> nm<sup>2</sup> for semiconducting SWNTs and 79.5 cm<sup>-1</sup> nm<sup>2</sup> for metallic ones.<sup>25</sup> For very small SWNTs, the splitting can be large which leads to a small  $\omega_G^-$ . For example,  $\omega_G^- \approx 1370$  cm<sup>-1</sup> for the *G*<sup>-</sup> mode of (4,2) semiconducting tube, which has been clearly identified.<sup>17</sup> Spectrum 0 in Fig. 3 shows the pristine *G*<sup>+</sup> Raman band. Four components, centered at 1558, 1586, 1599, and 1615 cm<sup>-1</sup>, can be identified. The three high-frequency components near the graphite-like *G* mode are attributed to *G*<sup>+</sup> modes of the three co-existing tubes. The contributions from different tubes are overlapped and indistinguishable. The component at 1558 cm<sup>-1</sup> is relatively broad and weak, which can be attributed to *E*<sub>1g</sub> or *E*<sub>2g</sub> modes from the three tubes.

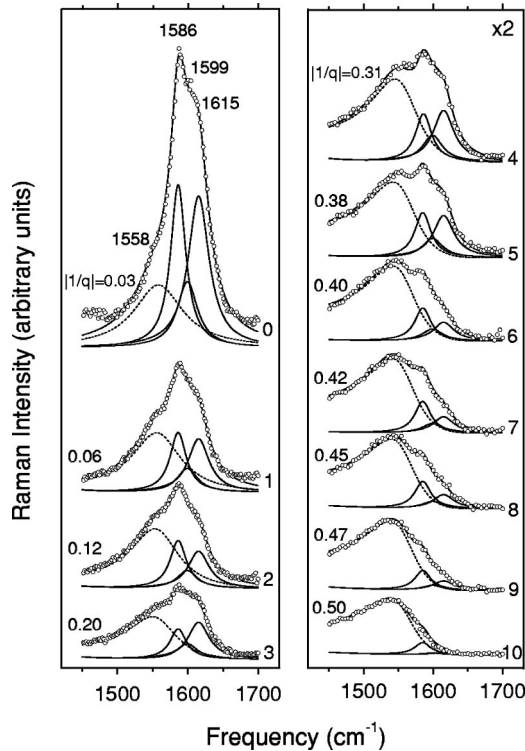


FIG. 3. Fitting results of Li doped 0.4-nm SWNTs. Open circles are experimental data. The solid curves are fitted Lorentzians, while dotted curves are the BWF components; from 0 to 10: pristine to saturated lithium doped sample. Peak frequencies are indicated on spectrum 0. The coupling constant ( $1/q$ ) is labeled on the left shoulder of each curve.

As shown in Fig. 3, we fit the line shape of different doping levels by three Lorentzians for three high-frequency peaks and one Breit-Wigner-Fano (BWF) line shape for the peak near  $1558\text{ cm}^{-1}$ . The BWF line shape is given by

$$I(\omega) = I_0 \frac{[1 + (\omega - \omega_{\text{BWF}})/q\Gamma]^2}{1 + [(\omega - \omega_{\text{BWF}})/\Gamma]^2}, \quad (2)$$

where  $I_0$ ,  $\omega_{\text{BWF}}$ , and  $\Gamma$  are, respectively, the intensity, renormalized frequency and broadening parameter.<sup>26</sup> The asymmetric line shape is governed by  $-1/q$  which characterizes the interaction between the discrete phonon state and electronic continuum.<sup>26</sup> We trace the line shapes of these  $G^+$  bands as a function of doping level. For the Lorentzians, the behavior can be described mainly by intensity competition with fixed line, width and center frequency. For the BWF component near  $1558\text{ cm}^{-1}$ , the variation is characterized by gradual changes of the line shape and downshift in frequency. Compared with three high-frequency Lorentzians, the intensity of the BWF component decreases in a much slower pace and survives till the highest doping level (spectrum 10). The peak at  $1558\text{-cm}^{-1}$  turns out to be the discrete phonon state coupled with the electronic continuum, which indicates the charge transfer from lithium atom to the SWNTs. The  $-1/q$  value of the BWF component increases from 0.03 to 0.50, leading to a downshift of the BWF peak from  $1558$  to  $1537\text{ cm}^{-1}$  and significant broadening in line

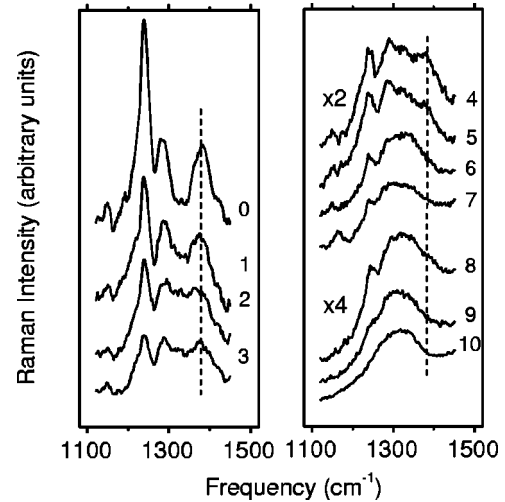


FIG. 4.  $D$  bands of lithium doped 0.4-nm SWNTs. From 0 to 10: pristine to saturated lithium doped sample. The dash lines denote the  $G^-$  Raman modes (Ref. 17).

shape. The  $-1/q$  value is larger than that reported for alkali-metal doped SWNT bundles,<sup>2</sup> but a factor of  $\sim 2$  smaller than that observed in the first stage alkali metal graphite-intercalated compounds ( $MC_8$ , where  $M$  is K, Cs, and Rb). Qualitatively, larger  $-1/q$  value indicates higher lithium doping concentration in the 0.4-nm SWNTs. The value of  $1/q$  is proportional to the density of electronic states at the Fermi level (in units of the number of states per eV per C atom).<sup>26</sup> We estimate, with elevating lithium concentration, electronic density of states increase significantly from 0.1 to 1.6 states/eV/C.

The frequency of BWF line shape in Fig. 3 is remarkably close to that observed in nanotubes with diameters of 1–2 nm.<sup>2,4</sup> The region near  $1550\text{ cm}^{-1}$  exhibits to be a general BWF region where coupling occurs between a discrete phonon mode and an electronic continuum. In large diameter tubes, due to small separation between  $G^+$  and  $G^-$  modes, the  $G^-$  band locates near the general BWF region and couples with the electronic continuum.<sup>26</sup> In our ultrasmall SWNTs, the  $G^-$  band is far away from the BWF region, instead the splitted  $G^+$  modes appear. It is the  $G^+$  mode that couples with the electronic continuum to form the BWF line. From this fact, we can see that the continuum spectra of plasmon and the discrete phonon line couple to form the BWF line by a general Fano effect. Fano effect does not specify the character of the discrete phonon mode, that is, both  $G^+$  and  $G^-$  modes can couple with the electronic continuum.

Recently, electrochemistry and stoichiometry have been utilized to prepare alkali-doped SWNTs.<sup>4,5</sup> In their Raman spectra, the  $G$  band upshifted at low doping level, but downshifted in saturated doping sample, and the RBM was found to be downshift with doping.<sup>5</sup> These behaviors are different from our work using the vapor phase adsorption method. In the electrochemistry method, influences from electrolytes are contributing factors to the Raman profile,<sup>4</sup> which are probably the origin of these discrepancies.

Below  $1450\text{ cm}^{-1}$ , rich Raman features in the pristine

spectrum have been explained by  $G^-$  mode around  $1370\text{ cm}^{-1}$  as well as contributions from phonon density of states of SWNTs and graphite.<sup>17</sup> As shown in Fig. 4, upon lithium doping, the  $D$ -band variation of doped 0.4-nm SWNTs can be summarized as follows: in low doping level, it has the same profile as the pristine sample. With lithium concentration increased, the  $D$  band features gradually merge into a broad band while decrease their intensities. No evident downshift of  $G^-$  lines is observed in spectrum 0–4. In contrast, the BWF line observed around  $1558\text{ cm}^{-1}$  shows significant downshift even at low doping level. Starting from moderate doping level, the  $G^-$  lines seem downshifted and broadened. This profile, however, should not result from the BWF effect, because the BWF band usually has an unsymmetrical line shape with high intensity at the low-frequency side and low intensity at the high-frequency side. A further

study is needed to identify the variation of  $G^-$  modes in the high doping level.

In summary, lithium was doped into 0.4-nm single-walled carbon nanotubes using the vapor phase adsorption method. In the measured Raman spectrum, the upshift of the RBM is attributed to the enhanced stiffness by insertion of lithium atoms; from line-shape fitting and analysis, variation of the  $G$  bands is attributed to the intensity competition between three Lorentzians and one BWF line shape. The region near  $1550\text{ cm}^{-1}$  turns out to be general for coupling between discrete phonon bands and the electronic continuum.

We are grateful to Professor P. Sheng and Professor C. T. Chan for stimulating discussions, and H. J. Liu for discussions and theoretical calculation. This research was supported by the CERC Grants from the Research Grants of Hong Kong. R. S. acknowledges a Grant-in-Aid (Grant No. 13440091) from the Ministry of Education, Japan.

\*Electronic address: phzktang@ust.hk

<sup>1</sup>R. Saito, G. Dresselhaus, and M. S. Dresselhaus, *Physical Properties of Carbon Nanotubes* (Imperial College Press, London, 1998).

<sup>2</sup>A.M. Rao, P.C. Eklund, S. Bandow, A. Thess, and R.E. Smalley, *Nature* (London) **388**, 257 (1997).

<sup>3</sup>R.S. Lee, H.J. Kim, J.E. Fischer, A. Thess, and R.E. Smalley, *Nature* (London) **388**, 255 (1997).

<sup>4</sup>A. Claye, S. Rahman, J.E. Fisher, A. Sirenko, G.U. Sumanasekera, and P.C. Eklund, *Chem. Phys. Lett.* **333**, 16 (2001).

<sup>5</sup>N. Bendiab, E. Anglaret, J.-L. Bantignies, A. Zahab, J.L. Sauvajol, P. Petit, C. Mathis, and S. Lefrant, *Phys. Rev. B* **64**, 245424 (2001).

<sup>6</sup>J. Zhao, A. Buldum, J. Han, and J.P. Lu, *Phys. Rev. Lett.* **85**, 1706 (2000).

<sup>7</sup>H. Shimoda, B. Gao, X.P. Tang, A. Kleinhammes, L. Fleming, Y. Wu, and O. Zhou, *Phys. Rev. Lett.* **88**, 015502 (2002).

<sup>8</sup>H. J. Liu and C. T. Chan (private communication).

<sup>9</sup>Y. Miyamoto, A. Rubio, X. Blase, M. Cohen, and S.G. Louie, *Solid State Commun.* **74**, 299 (1995).

<sup>10</sup>J. Yang, H.J. Liu, and C.T. Chan, *Phys. Rev. B* **64**, 085420 (2001).

<sup>11</sup>H.J. Liu and C.T. Chan, *Solid State Commun.* **125**, 77 (2003).

<sup>12</sup>N. Wang, Z.K. Tang, G.D. Li, and J.S. Chen, *Nature* (London) **408**, 50 (2000).

<sup>13</sup>S. Qiu, W. Pang, H. Kessler, and J.-L. Guth, *Zeolites* **9**, 440 (1989).

<sup>14</sup>P. Launois, R. Moret, D.L. Bolloc'h, P.A. Albouy, Z.K. Tang, G. Li, and J. Chen, *Solid State Commun.* **116**, 99 (2000).

<sup>15</sup>Z.M. Li *et al.*, *Phys. Rev. Lett.* **87**, 127401 (2001).

<sup>16</sup>H.D. Sun, Z.K. Tang, J.S. Chen, and G. Li, *Solid State Commun.* **109**, 365 (1999).

<sup>17</sup>A. Jorio *et al.*, *Chem. Phys. Lett.* **351**, 27 (2002).

<sup>18</sup>Z.K. Tang, L. Zhang, N. Wang, X.X. Zhang, G.H. Wen, G.D. Li, J.N. Wang, C.T. Chan, and P. Sheng, *Science* **408**, 50 (2000).

<sup>19</sup>J. Kurti, G. Kresse, and H. Kuzmany, *Phys. Rev. B* **58**, 8869 (1998).

<sup>20</sup>X. Blase, L.X. Benedict, E.L. Shirley, and S.G. Louie, *Phys. Rev. Lett.* **72**, 1878 (1994).

<sup>21</sup>H.J. Liu and C.T. Chan, *Phys. Rev. B* **66**, 115416 (2002).

<sup>22</sup>A. Jorio, G. Dresselhaus, M.S. Dresselhaus, M. Souza, M.S.S. Dantas, M.A. Pimenta, A.M. Rao, R. Saito, C. Liu, and H.M. Cheng, *Phys. Rev. Lett.* **85**, 2617 (2000).

<sup>23</sup>G.S. Duesberg, I. Loa, M. Burghard, K. Syassen, and S. Roth, *Phys. Rev. Lett.* **85**, 5436 (2000).

<sup>24</sup>M. Dresselhaus, G. Dresselhaus, A. Jorio, A.S. Filho, and R. Saito, *Carbon* **40**, 2043 (2002).

<sup>25</sup>A. Jorio *et al.*, *Phys. Rev. B* **65**, 155412 (2002).

<sup>26</sup>S.D.M. Brown, A. Jorio, P. Corio, M.S. Dresselhaus, G. Dresselhaus, R. Saito, and K. Kneipp, *Phys. Rev. B* **63**, 155414 (2001).